

# **CBMAP: Clustering-based manifold approximation and projection for dimensionality reduction**

Berat Doğan

Department of Biomedical Engineering, 44280, Battalgazi, Malatya, Türkiye

## **ABSTRACT**

Dimensionality reduction methods are employed to decrease data dimensionality, either to enhance machine learning performance or to facilitate data visualization in two or three-dimensional spaces. These methods typically fall into two categories: feature selection and feature transformation. Feature selection retains significant features, while feature transformation projects data into a lower-dimensional space, with linear and nonlinear methods. While nonlinear methods excel in preserving local structures and capturing nonlinear relationships, they may struggle with interpreting global structures and can be computationally intensive. Recent algorithms, such as the t-SNE, UMAP, TriMap, and PaCMAP prioritize preserving local structures, often at the expense of accurately representing global structures, leading to clusters being spread out more in lower-dimensional spaces. Moreover, these methods heavily rely on hyperparameters, making their results sensitive to parameter settings.

To address these limitations, this study introduces a clustering-based approach, namely CBMAP (**C**lustering-**B**ased **M**anifold **A**pproximation and **P**rojection), for dimensionality reduction. CBMAP aims to preserve both global and local structures, ensuring that clusters in lower-dimensional spaces closely resemble those in high-dimensional spaces. Experimental evaluations on benchmark datasets demonstrate CBMAP's efficacy, offering speed, scalability, and minimal reliance on hyperparameters. Importantly, CBMAP enables low-dimensional projection of test data, addressing a critical need in machine learning applications. CBMAP is made freely available at <https://github.com/doganlab/cbmap> and can be installed from the Python Package Directory (PyPI) software repository with the command *pip install cbmap*.

**Keywords:** dimensionality reduction, clustering, UMAP, TriMap, PaCMAP

## INTRODUCTION

The amount of data produced in different application areas, including health, finance, education, and social media, has significantly increased in recent years. Additionally, the size and dimension of the data being generated are also growing. The large dimensionality of the generated data poses several problems for machine learning techniques. The generalization ability of learning algorithms weakens in the presence of many features, especially if the number of data points is less than the number of dimensions, and overfitting occurs. This situation is called the curse of dimensionality in the literature. In addition, high dimensionality brings complexity in terms of computation.

Another disadvantage of high dimensionality is that it does not allow for visualization. On the other hand, data visualization is frequently required to obtain a deeper understanding of data. Therefore, the dimension of the data is reduced by using various dimension reduction methods, either to improve the performance of learning algorithms or to visualize the data by reducing the dimension to two- or three-dimensional space.

There are two fundamental approaches in the literature to reduce the data dimension. These two methods are known as “feature selection” and “feature transformation”. In feature selection methods [1], the most significant features are selected by considering a specific metric, and unimportant features are removed from the data set. Thus, the dimension is reduced without making any changes to the remaining feature values. In the feature transformation methods, the data is projected or transformed to a low-dimensional space, and the feature values are changed after transformation. Feature transformation methods can also be categorized into two groups, namely, linear and nonlinear methods. In linear methods (e.g., PCA [2] and LDA [3]), data is multiplied by a transformation matrix and projected into a low-dimensional space. Linear methods are usually computationally efficient and provide straightforward interpretations of global structures. However, these methods struggle with capturing nonlinear relationships and preserving local structures effectively. Nonlinear methods on the other hand are mostly manifold-based methods. Early examples of these methods are MDS [4], ISOMAP [5], LLE [6], and more recent examples include t-SNE [7], UMAP [8], TriMap [9], and PaCMAP [10]. In comparison to linear methods, these methods are known to better preserve local structures and capture nonlinear relationships in high-dimensional data, making them powerful for visualizing complex datasets. However, they can be computationally intensive and may suffer from difficulties in interpreting global structures.

One of the primary goals of dimensionality reduction algorithms is to preserve the inherent structure and relationships present in the high-dimensional data when mapping it to a lower-dimensional space. This includes preserving natural groupings or clusters of data points. When performing dimensionality reduction, the algorithm aims to retain as much relevant information as possible while reducing the number of dimensions. This involves capturing the essential patterns, relationships, and structures that exist in the high-dimensional space. If the algorithm is successful, the resulting lower-dimensional representation should maintain the key characteristics of the original data, including any natural groupings or clusters. Recent algorithms such as the t-SNE, UMAP, TriMap, and PaCMAP aim to preserve the local and global structure of the data as much as possible in the lower-dimensional space. However, these methods often prioritize maintaining the local structure by sacrificing some accuracy in representing the global structure, which can lead to clusters being spread out more in the lower-dimensional space. Although this usually helps for better visualization, the resulting lower-dimensional representations may not perfectly reflect the global arrangement of clusters present in the high-dimensional space. Moreover, the resulting representations are often highly dependent on the hyperparameters of these algorithms. t-SNE has the perplexity parameter, UMAP has the `n_neighbors`, TriMAP has the `n_inliers`, `n_outliers`, `n_random`, `weight_temp`, `weight_adj`, and `n_iters` and PaCMAP has the `FP_ratio` and `MN_ratio`. Another limitation of the t-SNE, TriMAP, and PaCMAP algorithms is that these algorithms could not provide a low-dimensional projection for the unseen samples (test dataset). Although the UMAP can provide a low-dimensional projection of the test dataset, the resulting clusters are not reliable as this method significantly distorts the cluster topologies and global arrangement of the clusters. Therefore, there is a need for a new algorithm that preserves both global and local structures to the greatest extent possible, ensuring that the clusters formed in the low-dimensional space closely resemble those in the high-dimensional space. Ideally, this new algorithm should be either parameter-free or have reduced reliance on hyperparameters and should also provide a low-dimensional projection of the test data. Additionally, given the large sizes of contemporary datasets, the algorithm should be scalable and computationally efficient.

Given the limitations highlighted above regarding the recent methods, this study introduces a novel approach, CBMAP (clustering-based manifold approximation and projection) for dimensionality reduction. CBMAP's primary objective is to retain the structural integrity of high-dimensional clusters post-dimensionality reduction. To achieve this goal, CBMAP initiates clustering within the high-dimensional space to determine cluster centers, which are

then utilized to compute membership values for each data point relative to these centers. Subsequently, during the data embedding process, CBMAP ensures that the membership values between low-dimensional cluster centers and data points mirror those obtained in the high-dimensional space. This methodology aids in preserving both the global data structure and the local cluster arrangement. Experimental evaluations conducted on diverse benchmark datasets showcased the algorithm's effectiveness compared to recent methods. CBMAP is characterized by its speed, scalability, and absence of hyperparameters that substantially impact algorithm behavior. Moreover, CBMAP allows for a low-dimensional projection of the test data which is highly desirable in the machine learning field.

## MATERIALS AND METHODS

### The CBMAP algorithm

Let  $X \in R^{n \times d}$  be the data matrix to be projected from high-dimensional to low-dimensional space, where  $n$  represents the number of data points and  $d$  represents the dimension in high-dimensional space. First, CBMAP clusters the data matrix  $X$  by using a clustering algorithm. The default clustering algorithm is the k-means algorithm. However, depending on the data structure one could select another clustering method that best fits the data. Let  $C^H \in R^{k \times d}$  be the cluster centers provided by the clustering algorithm in high-dimensional space, where  $k$  represents the number of clusters. Next, in the high-dimensional space, the membership of each data point  $x_i \in X$ ,  $i = 1, 2, \dots, n$  to each cluster center  $c_j^H \in C^H$ ,  $j = 1, 2, \dots, k$  is computed with Eq.1.

$$u_{ij}^H = \exp\left(-\frac{d_{ij}^2}{2\sigma_H^2}\right) \quad i = 1, 2, \dots, n \quad j = 1, 2, \dots, k \quad (1)$$

In Eq.1,  $u_{ij}^H$  represents the membership of a data point  $x_i$  to the cluster center  $c_j^H$  in high-dimensional space.  $d_{ij} = \|x_i - c_j^H\|$  is the Euclidean distance between the data point  $x_i$  and the cluster center  $c_j^H$  and  $\sigma_H$  is the average of the median values of the data points to cluster distances in high-dimensional space. Thus, a membership matrix  $U^H \in R^{n \times k}$  can be formed with the help of the computed  $u_{ij}^H$  membership values. The CBMAP algorithm aims to find the optimal projection  $Y \in R^{n \times m}$ ,  $m < d$  of the high-dimensional data such that, the membership matrix  $U^L \in R^{n \times k}$  computed in the low-dimensional space with the help of the low-dimensional cluster centers  $C^L \in R^{k \times m}$  minimizes the Frobenius norm provided in Eq.2.

$$F = \|U^L - U^H\| = \left( \sum_{i=1}^n \sum_{j=1}^k (u_{ij}^L - u_{ij}^H)^2 \right)^{1/2} \quad (2)$$

In Eq.2,  $u_{ij}^L$  represents the membership of a data point  $x_i$  to the cluster center  $c_j^L$  in low-dimensional space. The low-dimensional cluster centers  $C^L \in R^{k \times m}$  are obtained by the projection of high-dimensional cluster centers  $C^H \in R^{k \times d}$  with the help of the PCA or by random initialization.  $u_{ij}^L$  values can be computed as in Eq.3.

$$u_{ij}^L = \exp\left(-\frac{d_{ij}^2}{2\sigma_L^2}\right) \quad i = 1, 2, \dots, n \quad j = 1, 2, \dots, k \quad (3)$$

In Eq.3,  $d_{ij} = \|y_i - c_j^L\|$  is the Euclidean distance between the data point  $y_i$  and the cluster center  $c_j^L$  and  $\sigma_L$  is the average of the median values of the between-cluster distances in low-dimensional space.

Each  $y_i \in Y$ ,  $i = 1, 2, \dots, n$  data point in low-dimensional space can be optimally embedded around the low-dimensional cluster centers. For this purpose, the Frobenius norm  $F$  needs to be derived for each  $y_i$  to find the loss function that will be used in the optimization process.

$$\frac{\partial F}{\partial y_{il}} = \frac{\partial F}{\partial u_{ij}^L} \cdot \frac{\partial u_{ij}^L}{\partial y_{il}} \cdot \frac{\partial d_{ij}}{\partial y_{il}}, \quad i = 1, 2, \dots, n \quad l = 1, 2, \dots, m \quad (4)$$

The Eq.4 applies the chain-rule to compute the derivative of  $F$  with respect to each dimension  $l = 1, 2, \dots, m$  of a data point  $y_i$ . The first term of the chain can be computed as in Eq.5.

$$\frac{\partial F}{\partial u_{ij}^L} = \frac{1}{2} \cdot \frac{1}{\|U^L - U^H\|} \cdot 2 \cdot (u_{ij}^L - u_{ij}^H) = \frac{u_{ij}^L - u_{ij}^H}{\|U^L - U^H\|} = \frac{u_{ij}^L - u_{ij}^H}{F} \quad (5)$$

While the second term of the chain can be computed as in Eq.6.

$$\frac{\partial u_{ij}^L}{\partial d_{ij}} = -\frac{d_{ij}}{\sigma_L^2} \cdot \exp\left(-\frac{d_{ij}^2}{2\sigma_L^2}\right) \quad (6)$$

Finally, the third term of the chain can be computed as in Eq.7.

$$\frac{\partial d_{ij}}{\partial y_{il}} = \frac{y_{il} - c_{jl}^L}{d_{ij}} \quad (7)$$

Thus, by combining Eq.5, Eq.6, and Eq.7 the derivative of  $F$  with respect to  $y_{il}$  can be computed as in Eq.8.

$$\frac{\partial F}{\partial y_{il}} = -\frac{u_{ij}^L - u_{ij}^H}{F} \cdot \exp\left(-\frac{d_{ij}^2}{2\sigma_L^2}\right) \cdot \frac{y_{il} - c_{jl}^L}{\sigma_L^2} \quad (8)$$

A step-by-step description of the CBMAP algorithm is also provided in Algorithm 1.

**Algorithm 1:** A description of the CBMAP algorithm.

**Data:** dataset  $X \in R^{n \times d}$

clustering method parameters: method (default k-means), n\_cluster

optimization parameters: max\_iter, learning\_rate

**Result:** low-dimensional data representation  $Y \in R^{n \times m}$

**begin**

Cluster the  $X \in R^{n \times d}$  high-dimensional data by a clustering algorithm (default k-means) and find the cluster centers  $C^H \in R^{k \times d}$  and cluster labels.

Calculate the  $\sigma_H$  value by computing the average of the median value of data point to cluster center distances in high-dimensional space.

Compute the membership values of each data point  $x_i$  to the cluster center  $c_j^H$  as in Eq.1 and form the  $U^H \in R^{n \times k}$  membership matrix in high-dimensional space.

Use the PCA to project the high-dimensional cluster centers  $C^H \in R^{k \times d}$  into low-dimensional space to obtain the  $C^L \in R^{k \times m}$  and apply standard normalization to  $C^L \in R^{k \times m}$ .

Calculate the  $\sigma_L$  value by computing the average of the median value of between-cluster distances in low-dimensional space.

Generate random  $y_i \in Y$ ,  $i = 1, 2, \dots, n$  data points around the cluster centers  $c_j^L \in C^L$ . Use the cluster labels to create random data points around their own cluster center.

**for** iter=1 **to** max\_iter **do**

    Compute the membership values of each data point  $y_i$  to the cluster center  $c_j^L$  as in Eq.3 and form the  $U^L \in R^{n \times k}$  membership matrix in high-dimensional space.

    By using the loss function provided in Eq.7, use the adam optimization method to update the  $y_i \in Y$  positions.

    Update the cluster centers by taking the average of data points assigned to each cluster and apply standard normalization to the updated cluster centers.

    Update the  $\sigma_L$  value with the newly computed cluster centers.

**end**

**end**

## Experimental datasets

The CBMAP algorithm was tested with several benchmark toy and real-world datasets. Toy datasets include the S-curve dataset, Sphere dataset, Swiss-roll dataset, and the Mammoth dataset [11]. Among these S-curve [12] and Swiss-roll [13] datasets were generated by utilizing python scikit-learn library. For the S-curve dataset the sklearn.datasets.make\_s\_curve function and for the Swiss-roll dataset the sklearn.datasets.make\_Swiss\_roll function was used. The Sphere dataset was generated according to the example provided in [14]. In addition, a new toy dataset (the Cuboids dataset) was also created to show the recent methods mostly fail to preserve the cluster topology and between-cluster distances after dimension reduction. Figure 1 shows the toy datasets used in the experiments.

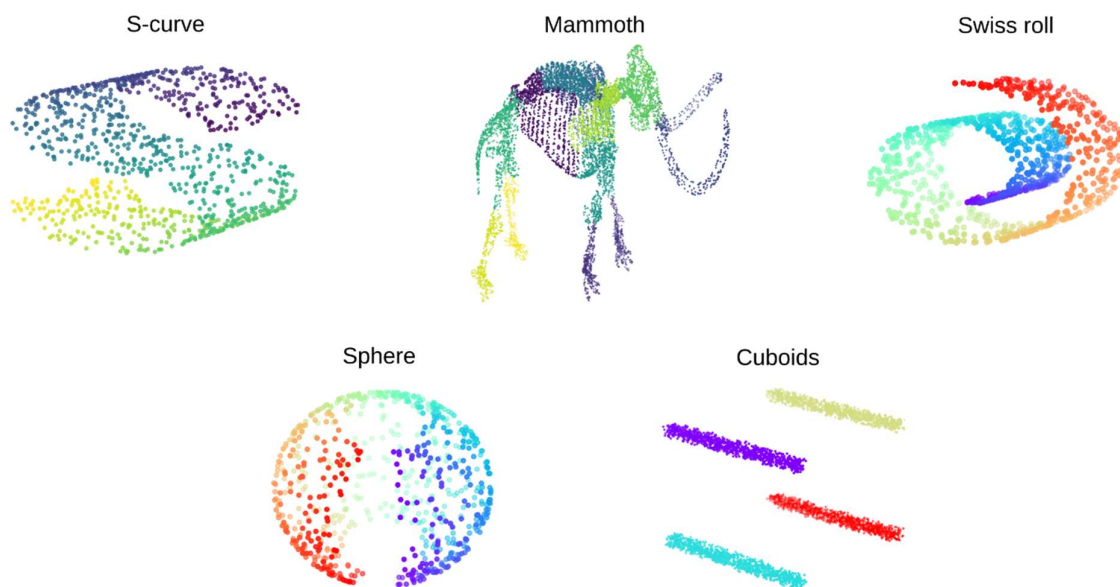


**Figure 1.** Toy datasets used in the experiments

Real-world datasets include the Iris dataset [3], COIL-20 [15], MNIST [16], Fashion MNIST [17], and a single-cell RNA-seq dataset, Duo 4Eq [18-20]. A description of the real-world datasets is provided in Table 1.

**Table 1.** A description of the real-world datasets used in the experiments.

Name	Size	Description
Iris	150×4	Three species of Iris flower (Iris setosa, Iris virginica and Iris versicolor) each consists of 50 samples. Four features were measured from each sample: the length and the width of the sepals and petals, in centimeters.
COIL-20	1440×1024	Gray-scale images of 20 objects in uniformly sampled orientations (5 degrees of rotation, 72 images per object). The size of each image is 32×32 pixels. Thus, each image is represented by a 1024-dimensional feature vector.
MNIST	70000×784	Images of handwritten digits (0–9) of size 28×28 each represented by a 784-dimensional feature vector.
Fashion MNIST	70000×784	Gray-scale images of clothing items such as t-shirt, pullover, bag, etc. of size 28×28 each represented by a 784-dimensional feature vector.
Duo 4Eq scRNA-seq	3994x100	Randomly selected B-cells, CD14 monocytes, naive cytotoxic T-cells, and regulatory T-cells were combined and filtered considering the average expression (log normalized), variability, and dropout effects. Next, the dimension is further reduced by PCA to 100.

## **Parameter settings of the algorithms**

For a fair comparison of algorithms, each algorithm was run with its default parameters. The t-SNE has a default perplexity parameter of 30 and the maximum number of iterations  $n\_iter = 1000$ . In UMAP, the default value of the  $n\_neighbors$  is 15, and the default value of  $min\_dist = 0.1$ . For the TriMAP, the default value of  $n\_inliers = 12$ ,  $n\_outliers = 4$ ,  $n\_random = 3$ ,  $weight\_temp = 0.5$ ,  $weight\_adj = 500.0$ , and  $n\_iters = 400$ . For the PaCMAP, the default value of  $n\_neighbors = 10$ ,  $MN\_ratio = 0.5$ ,  $FP\_ratio = 2$ ,  $init = \text{“random”}$ , and  $num\_iters = 450$ . Finally, for the CBMAP algorithm, the default value of  $max\_iter = 500$ ,  $center\_init = \text{“PCA”}$  and  $clustering\_method = \text{“kmeans”}$ . The CBMAP algorithm also has the parameter  $n\_cluster$  (number of clusters), which does not have a default value and therefore must be specified. For a fair comparison, for small datasets with less than 5000 samples, the value of  $n\_clusters$  was chosen as 20, while for larger datasets with more than 5000 samples, the value of  $n\_clusters$  was chosen as 40.

## **Performance metrics**

In [9] authors proposed a method to quantify the global accuracy of the dimension reduction methods which focuses on the accuracy of the embedding in reflecting the global structure of the data similar to PCA. The global score (GS) of the PCA is 1, and the GS values close to one indicate a higher capacity of the method to reflect the global structure of the data. To quantify the local accuracy of the methods the k-nearest neighbor classification ( $k=3$ ) algorithm is utilized. A higher classification accuracy of the projected data suggests a better performance of the dimension reduction method.

## **Computational environment**

The CBMAP algorithm was implemented in Python. The algorithms were executed on a Dell Precision T7820 workstation equipped with two Intel Xeon® Silver 4210R 2.40GHz 20 core processors and 128 GB RAM.

## **RESULTS AND DISCUSSION**

### **CBMAP retains the cluster topology and relative positions of the clusters to one another after dimensionality reduction**

The recent methods often struggle to maintain both the cluster topology and the relative positions of clusters to one another following dimensionality reduction. To further confirm this observation, a new toy dataset, termed the Cuboids dataset (depicted in Figure 1), was created

for this study. This dataset comprises four clusters of cuboids formed via uniform distribution in three-dimensional space. It was hypothesized that recent methods would fail to preserve the sharp corners of the cuboids and inter-cluster distances post-dimensionality reduction. Experimental results conducted on this dataset are illustrated in Figure 2. In Figure 2, the clusters of the Cuboids dataset were gradually brought closer together (top panel), and dimension reduction was applied accordingly. Despite attempts to decrease the distance between cuboids, the outcomes yielded by t-SNE, UMAP, TriMap, and PaCMAP algorithms remained similar until the clusters were nearly overlapping. Once again, these methods failed to maintain the global structure of the clusters and distorted the cuboids' sharp corners. The resulting pairs of global scores (GS) and k-nearest neighbors classification accuracy (ACC) outcomes for each method validate the shortcomings of t-SNE, UMAP, TriMap, and PaCMAP algorithms in preserving the data's global structure. Conversely, CBMAP's GS closely mirrors that of PCA, and as the clusters are brought closer together, CBMAP effectively adjusts by providing closer embeddings in the low-dimensional space.

### **CBMAP's ability to preserve local and global structural details was further confirmed by well-known benchmark toy datasets**

The ability of algorithms to preserve both global and local structural details was further investigated using several well-known benchmark datasets (see Figure 1). Figures 3 depict the outcomes for the S-curve, Mammoth, Swiss roll, and Sphere datasets. These figures illustrate that recent methods struggle to identify the two-dimensional manifolds within these datasets. Conversely, the CBMAP algorithm successfully captures both global and local structural details in both the S-curve and Mammoth datasets. The results obtained through the CBMAP algorithm closely resemble those derived from PCA. However, unlike PCA projections, CBMAP also encompasses local structural details. For instance, in the Mammoth dataset, clear observations of ribs and both tusks are possible, whereas PCA projections only offer a global structure, abstracting the details of the ribs and omitting one of the tusks. For the Swiss roll and Sphere datasets, once more CBMAP outperforms the other methods by accurately preserving both global and local structural details, while the other methods struggle to identify the two-dimensional manifolds within these datasets. The recently proposed methods could also provide better results with certain parameter values. However, it is not possible to know beforehand which parameter values provide better results for any dataset and a successful algorithm should provide reasonable results even with its default parameters.

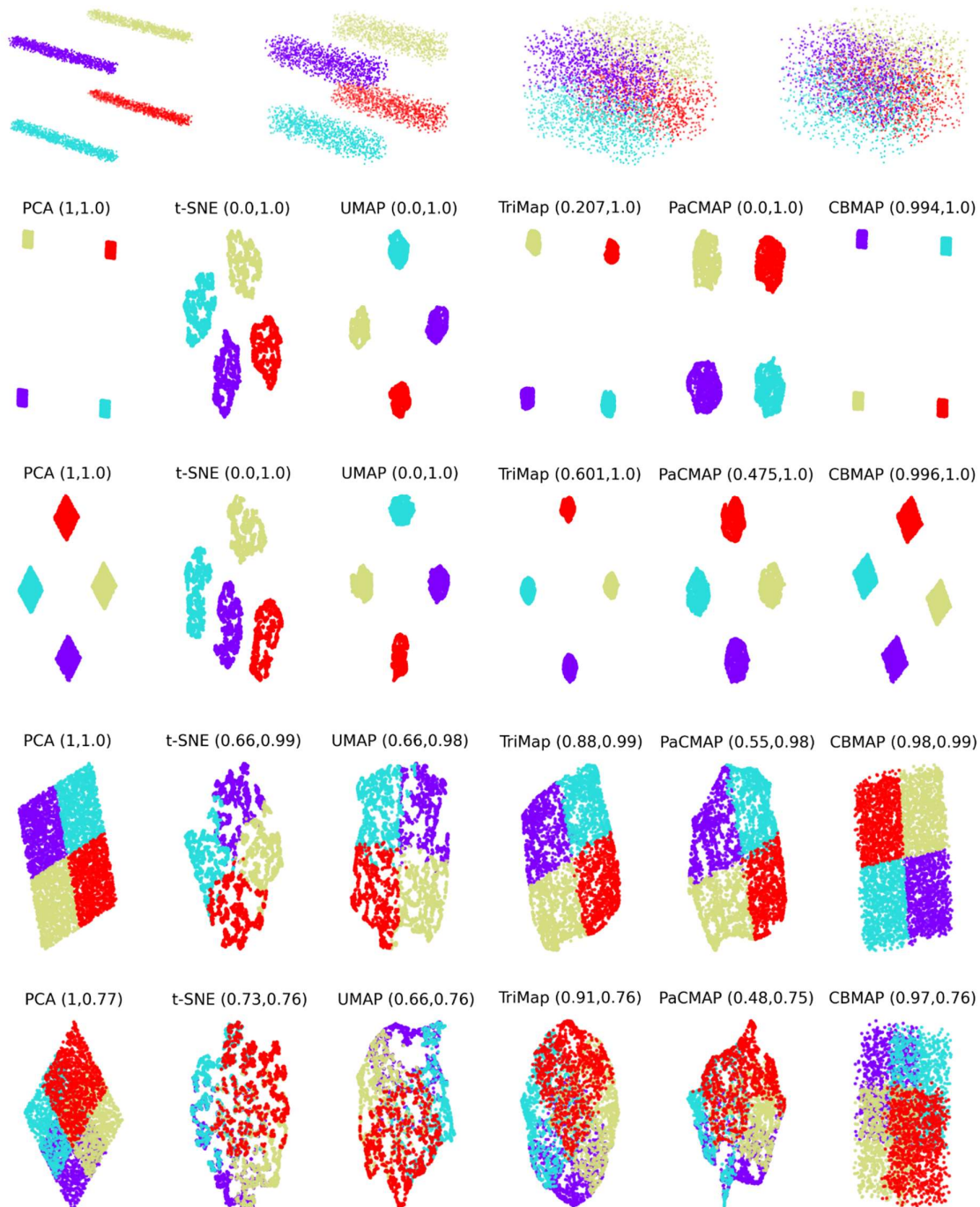


**Figure 2.** The Cuboids dataset's clusters are moved closer together (top panel) to assess how algorithms respond to changes in inter-cluster distances. PCA and CBMAP adeptly track these alterations, whereas other algorithms only capture the change when clusters are nearly overlapping. Additionally, PCA and CBMAP effectively retain the cuboids' sharp corners, whereas other algorithms fail to do so.

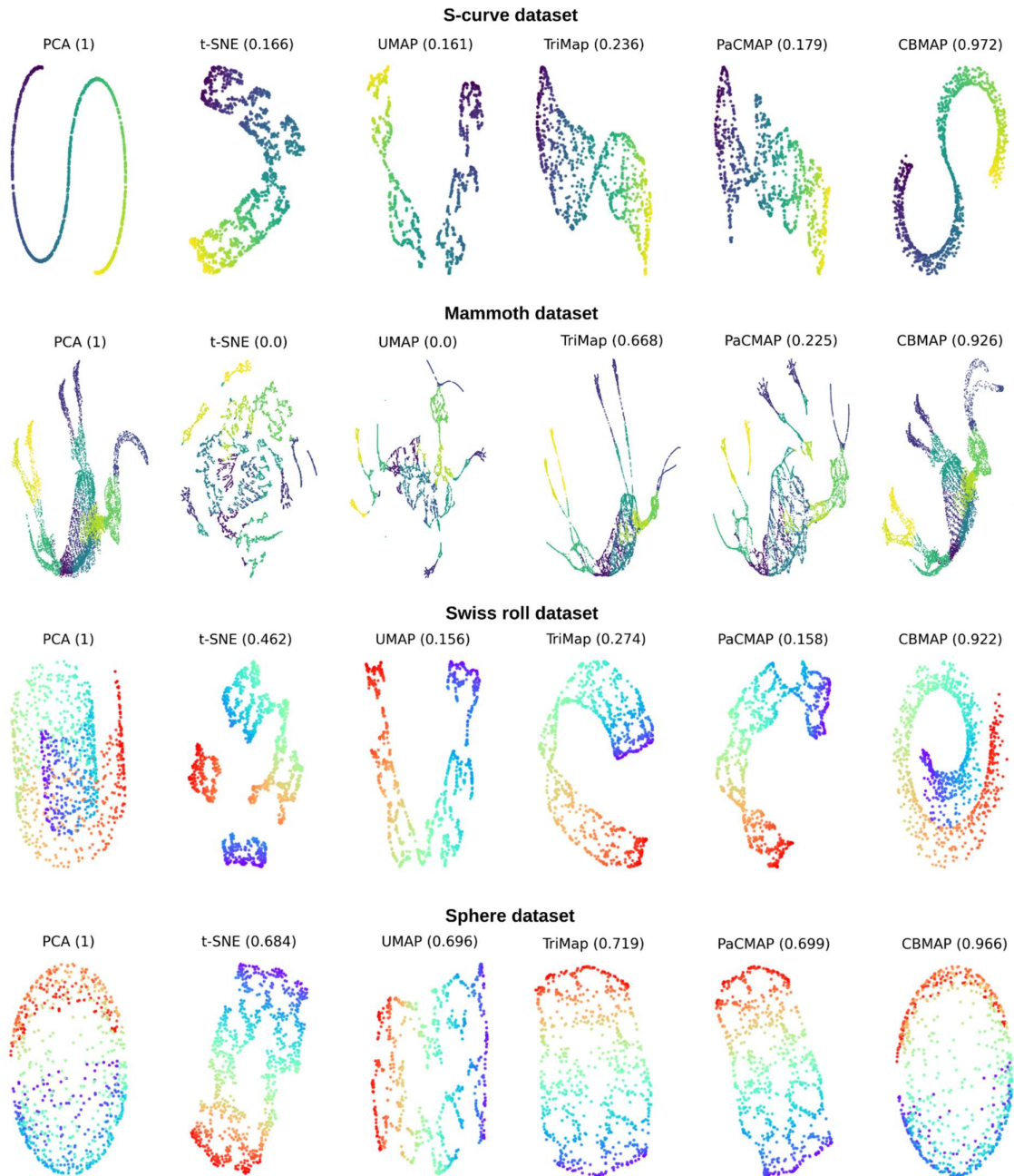


**Figure 3.** The CBMAP algorithm outperforms all of the algorithms in terms of the global score (GS). In comparison to the structures found by the PCA, the CBMAP algorithm provides further details. For example, in the Mammoth dataset, clear observations of ribs and both tusks are possible, whereas PCA projections only offer a global structure, abstracting the details of the ribs and omitting one of the tusks.

### CBMAP's performance on real-world benchmark datasets

One of the real-world datasets used to evaluate the performances of the methods is the well-known Iris dataset. This dataset comprises three clusters, with two clusters situated close to each other and the third cluster positioned farther away. Figure 4 displays the low-dimensional embeddings of the Iris data generated using various methods. The t-SNE, UMAP, TriMAP, and

PaCMAP methods notably distort the cluster topology, thus resulting in inferior performance in terms of GS. However, since the clusters do not overlap, the ACC scores are high for all methods. In the case of the Coil-20 dataset, CBMAP once again exhibits the highest GS and improves the ACC score compared to PCA. Conversely, recent methods outperform PCA and CBMAP in terms of ACC scores for other datasets. It is widely acknowledged that some level of information loss is expected after dimensionality reduction. As previously demonstrated with the Cuboids datasets, the higher ACC scores offered by these methods stem from their inclination to preserve local structure. While this may positively impact the ACC scores, it causes these methods to lag behind the CBMAP algorithm in terms of GS.

### **CBMAP allows dimensionality reduction for unseen test data**

A dimensionality reduction technique capable of reducing dimensions for unseen test data streamlines efficiency by eliminating the need to independently reduce the dimensionality of training and test datasets. This is particularly vital in scenarios demanding real-time or online learning, where consistency in dimensionality reduction processes for incoming test data is crucial. Consequently, models trained on reduced-dimensional representations can be seamlessly applied to new data without the need for additional preprocessing steps, thus enhancing the scalability and usability of machine-learning solutions in real-world contexts.

Of the compared methods, only PCA, UMAP, and CBMAP facilitate dimensionality reduction for unseen test data. While UMAP's well-separated clusters may yield superior results for visualization purposes, the reliability of its embeddings has been called into question, as evidenced in Figures 2-4. Therefore, when dimensionality reduction of unseen test data is imperative, the CBMAP algorithm emerges as a superior alternative to PCA. As depicted in Figure 4, CBMAP effectively preserves the global structure of the data while delivering higher accuracy (ACC) scores, a crucial requirement for machine-learning applications.

Experiments were carried out on both the Swiss roll and the MNIST datasets to illustrate how the PCA, UMAP, and CBMAP algorithms reduced the dimensionality of the test data. Initially, these datasets were split into training and test sets. Subsequently, parameters derived from the training set were applied to reduce the dimensionality of the test set. CBMAP employs  $C^H \in R^{k \times d}$  and  $C^L \in R^{k \times m}$  matrices, along with the  $\sigma_H$  and  $\sigma_L$  values, for this purpose. With these parameters derived from the training data, the embeddings for the test data can be optimally obtained in the low-dimensional space. As shown in Figure 5, the resulting embeddings of the test datasets for all three methods closely match those achieved with the training datasets.

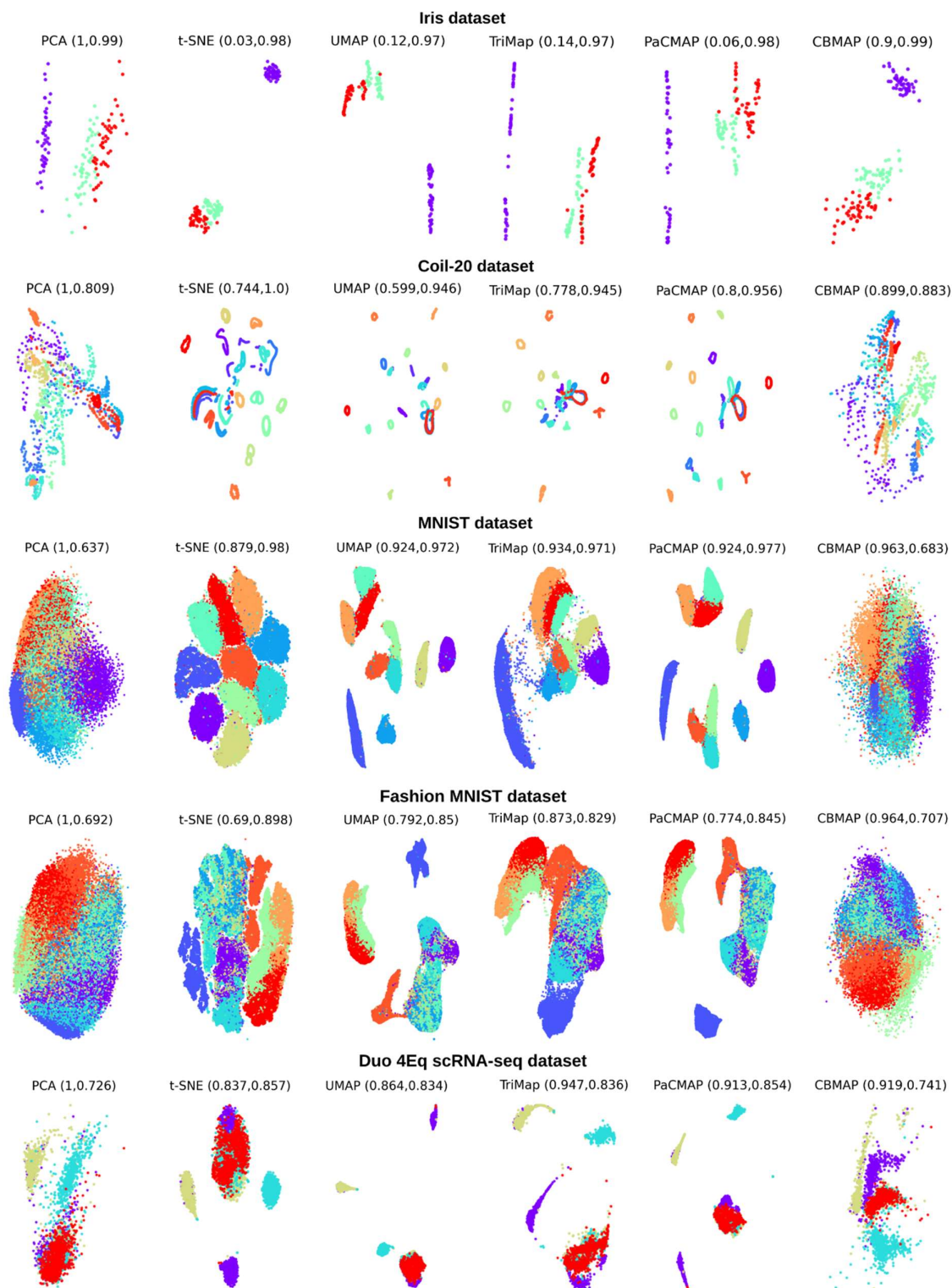


**Figure 4.** Experiments conducted on real-world datasets revealed that the t-SNE, UMAP, TriMap, and PaCMAP methods alter the overall structure of the data, resulting in lower GS scores compared to the CBMAP method. However, due to their tendency to retain local structure, these methods yield higher ACC scores than the CBMAP method.

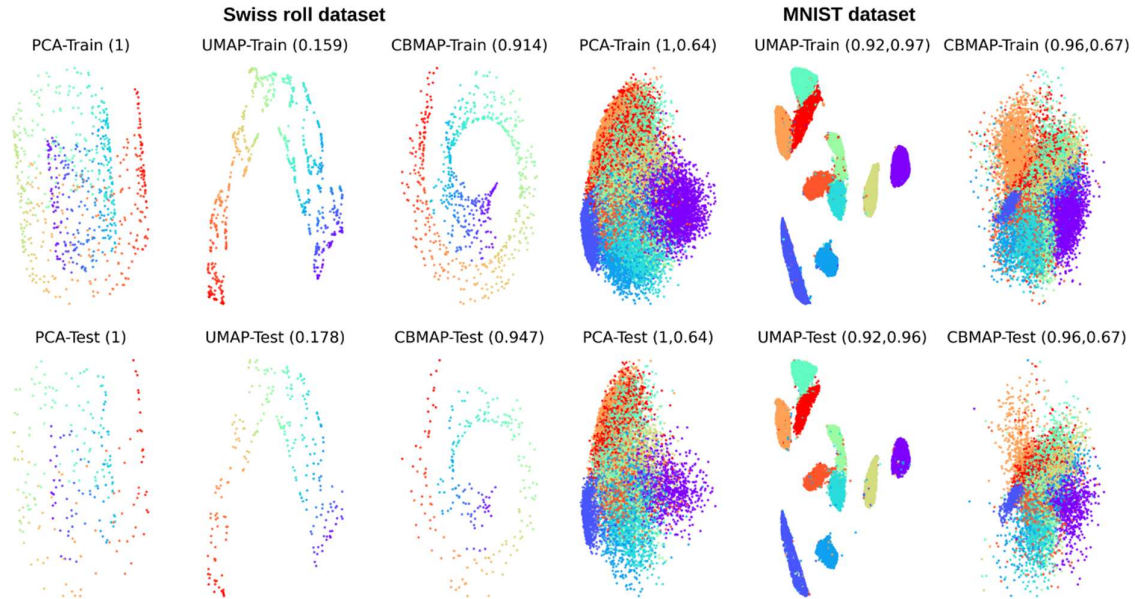


**Figure 5.** The embeddings obtained by CBMAP with the test datasets closely match those achieved with the training datasets.

To further evaluate the performance of the PCA, UMAP, and CBMAP methods on unseen test data, another series of experiments was conducted. In these experiments, the number of components (`n_components`) was varied to 2, 5, 10, 15, and 20 during dimensionality reduction for each method. Subsequently, the resulting embeddings of the test data were classified using a k-nearest neighbor classifier. Table 2 presents the average accuracy results from ten different trials. The table illustrates that UMAP yields comparatively higher results in two-dimensional space for each dataset. However, these results remain nearly constant as the number of components increases, which is not reasonable. In contrast, both PCA and CBMAP exhibit significant improvements in results with increased dimensionality. Moreover, in most cases, these methods outperform UMAP.

**Table 2.** k-nearest neighbor classification results of test datasets for the different values of “number of components”.

Datasets	Methods	Number of components (n components)				
		2	5	10	15	20
Coil-20	PCA	0.805	0.944	0.975	0.977	0.983
	UMAP	0.901	0.915	0.918	0.917	0.917
	CBMAP	0.797	0.942	0.965	0.972	0.958
MNIST	PCA	0.639	0.842	0.950	0.972	0.977
	UMAP	0.958	0.960	0.960	0.960	0.960
	CBMAP	0.673	0.853	0.939	0.959	0.963
Fashion MNIST	PCA	0.691	0.825	0.872	0.884	0.889
	UMAP	0.843	0.865	0.865	0.865	0.865
	CBMAP	0.702	0.834	0.864	0.871	0.868
Duo 4Eq scRNA-seq	PCA	0.730	0.874	0.893	0.889	0.885
	UMAP	0.835	0.862	0.858	0.858	0.860
	CBMAP	0.760	0.818	0.875	0.875	0.860

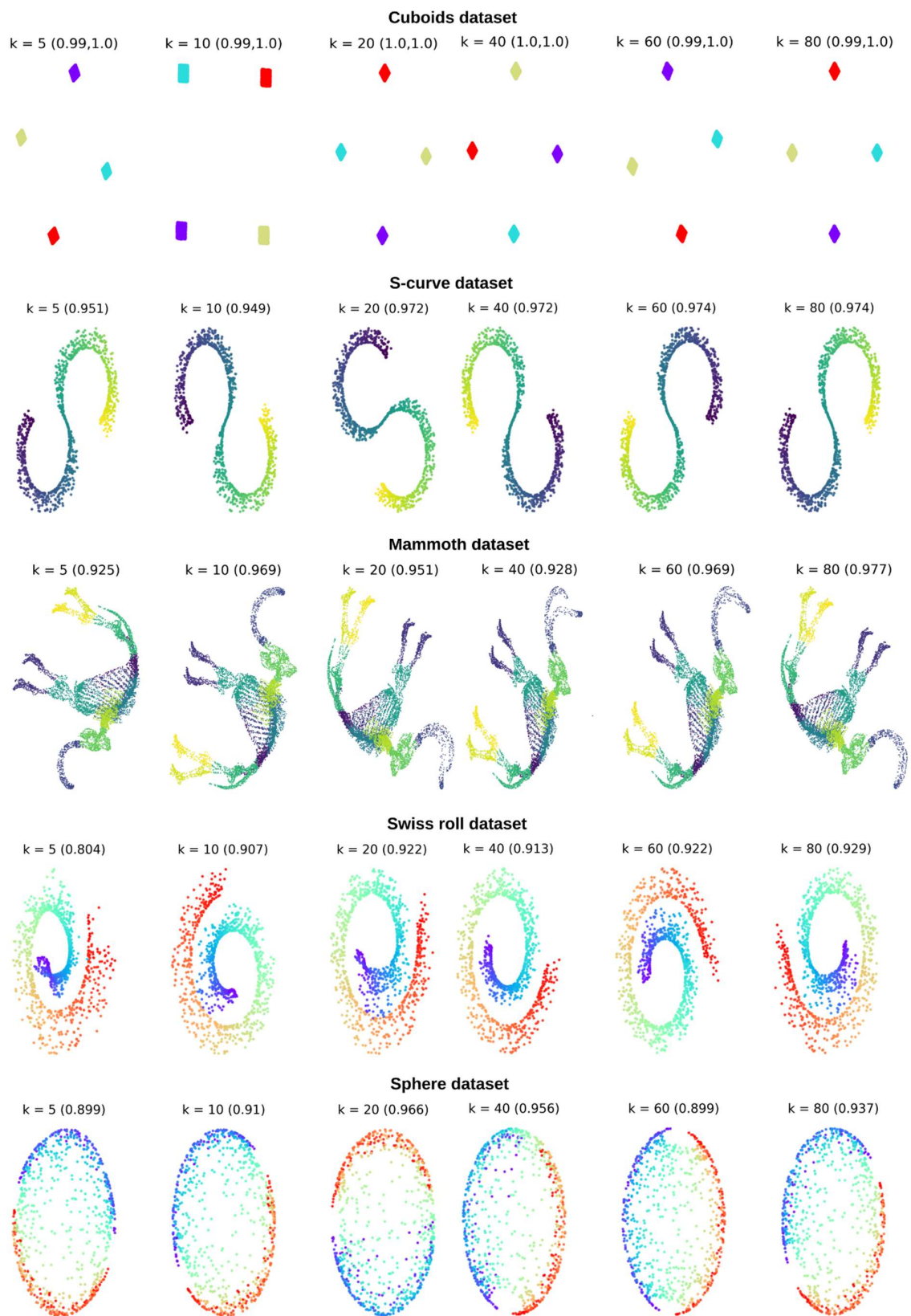


**Figure 6.** Increasing the number of clusters ( $k$ ) typically enhances the GS with toy datasets.

## **CBMAP's performance on different parameter settings**

### *Number of clusters*

In previous experiments, to ensure fairness in comparison, the number of clusters ( $k$ ) was established as 20 for datasets containing fewer than 5000 samples and 40 for datasets with over 5000 samples. While CBMAP consistently delivers robust projections with various  $k$  values, increasing the number of clusters typically improves the GS. To illustrate the influence of cluster numbers on CBMAP's performance, a series of experiments with different  $k$  values (5, 10, 20, 40, 60, 80) were conducted. Results are illustrated in Figure 6 for toy datasets and Figure 7 for real-world datasets.

Figure 6 demonstrates that even with  $k = 5$ , the s-curve dataset produces satisfactory results, achieving a GS of 0.951. As the number of clusters rises, the algorithm exhibits enhanced GS outcomes. Similarly, for the Mammoth dataset,  $k = 5$  yields satisfactory results, with a GS of 0.925. However, for this dataset, clear observation of the Mammoth's two tusks is only apparent with  $k = 20$  and  $k = 40$ . Likewise, for the Swiss roll and Sphere datasets,  $k = 5$  provides satisfactory results, and the GS scores increase with more clusters. For the Cuboids dataset, even with  $k = 5$ , the GS is notably high at 0.99, and the ACC score remains at 1.0 across all cases.

In Figure 7, for real-world datasets, the GS increases with more clusters. For the Coil-20 and MNIST datasets,  $k = 5$  yields a relatively lower GS. This is because the actual number of classes in these datasets exceeds 5, causing CBMAP to split the data into three clusters for the MNIST datasets. However, this is not the case for the Coil-20 dataset, where the resulting embedding remains satisfactory.

### *Initialization method*

In CBMAP, the initialization of low-dimensional cluster centers can be achieved either through the projection of high-dimensional cluster centers by PCA or through random initialization. Previous experiments utilized PCA-initialized cluster centers. To investigate the impact of random initialization, another series of experiments was conducted. Once again, the number of clusters was set as 20 for datasets containing fewer than 5000 samples and 40 for datasets containing more than 5000 samples. The results are illustrated in Figure 8.

As depicted in this figure, although there is a slight decrease in GS for the Mammoth dataset, the overall outcomes closely resemble those obtained with the PCA-initialized experiments. Hence, it can be inferred that the center initialization method has only a minor effect on the

results provided by CBMAP. Nonetheless, PCA initialization is recommended for ensuring rapid convergence of the algorithm towards an optimal solution.

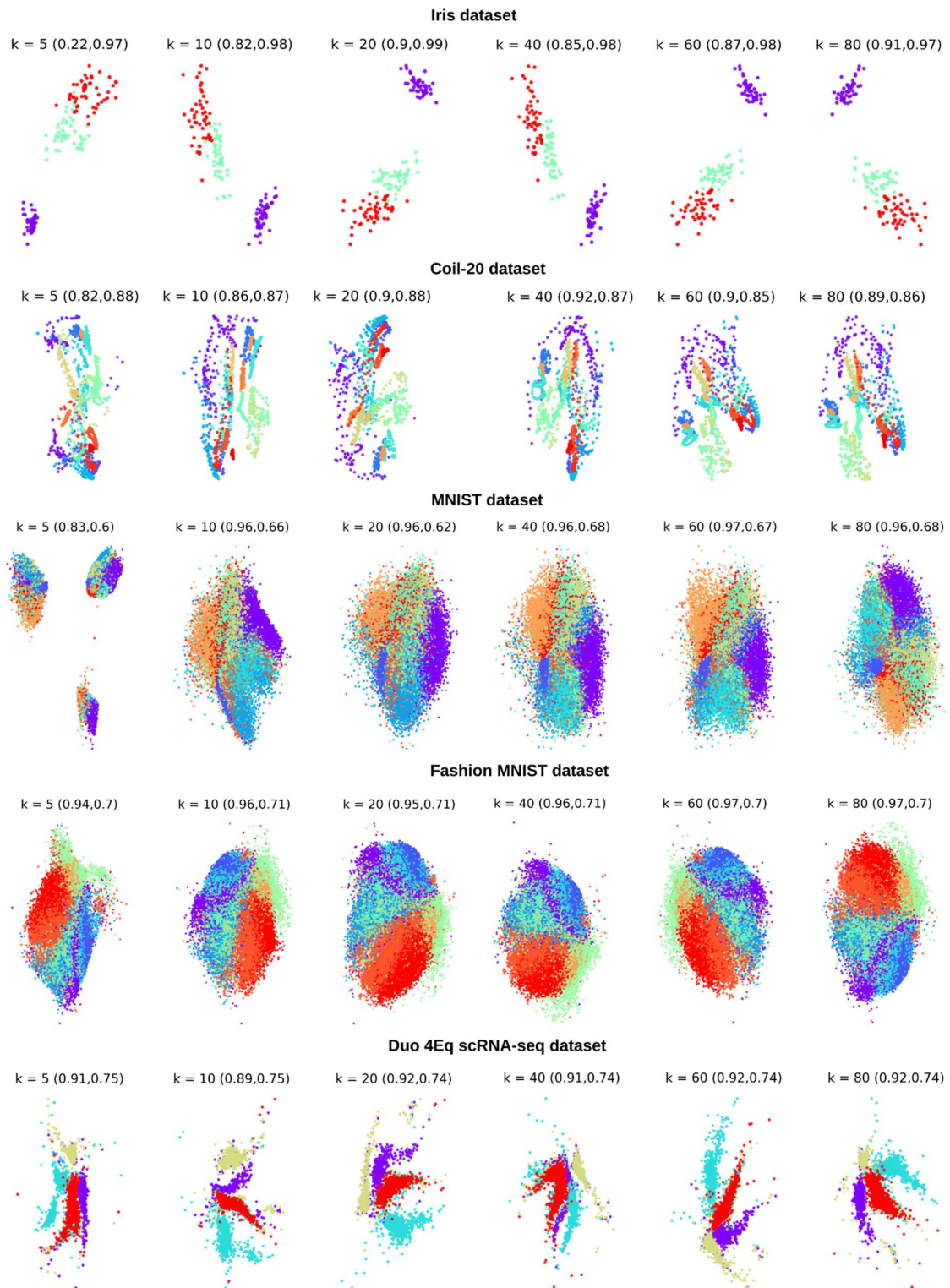


**Figure 7.** Increasing the number of clusters (k) typically enhances the GS, while it mostly does not affect the ACC score with real-world datasets.

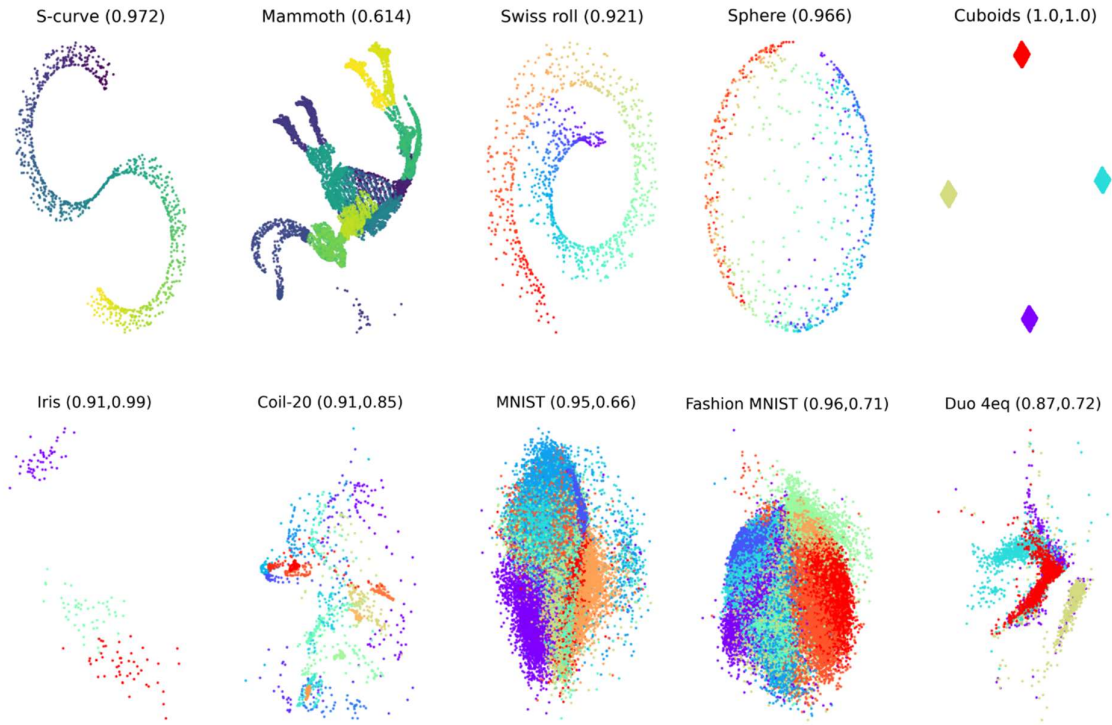


**Figure 8.** Random initialization of low-dimensional cluster centers has minor effects on the resulting embeddings of both the toy and real-world datasets.

### **CBMAP is computationally efficient**

Table 3 compares the computational time needed to conduct each experiment for the CBMAP dataset with that of other methods. In this comparison, the number of clusters was once again set to 20 for datasets with fewer than 5000 samples and 40 for datasets with more than 5000 samples. The Cuboids dataset measures 4000x3 in size, the Mammoth dataset 10000x3, and the Sphere dataset 720x3. The sizes of the s-curve and Swiss roll datasets are both 1000x3. The sizes of the real-world datasets were previously outlined in Table 1. All datasets were projected into two-dimensional space, as depicted in Figures 3 and 4. Being a linear algebra-based method, PCA is the fastest algorithm.

As indicated in Table 3, CBMAP demonstrates faster processing times compared to t-SNE and UMAP and is comparable with TriMap and PaCMAP for smaller datasets. However, for larger datasets like MNIST and Fashion MNIST, CBMAP is faster than t-SNE but slower than other recent methods. The clustering algorithm within CBMAP, which requires significant time to locate cluster centers in high-dimensional space, accounts for the slower processing times for these datasets. Despite utilizing the MiniBatchKmeans algorithm, which is designed for efficiency, CBMAP can still be relatively slow with large datasets. Nevertheless, overall, the computational time remains acceptable, and CBMAP proves sufficiently fast in generating low-

dimensional embeddings for large datasets. Furthermore, given the performance of the CBMAP algorithm with fewer clusters, as depicted in Figures 6 and 7, it can be inferred that the algorithm could generate the necessary embeddings even more rapidly.

**Table 3.** Computational time required for each method to project datasets into two-dimensional space.

	<b>Time elapsed for each method (sec)</b>					
<b>Datasets</b>	<b>PCA</b>	<b>t-SNE</b>	<b>UMAP</b>	<b>TriMap</b>	<b>PaCMAP</b>	<b>CBMAP</b>
Cuboids	0.017093	10.390414	11.859233	4.563494	2.893685	3.976686
S-curve	0.002586	2.359065	4.097905	1.433038	0.727454	0.952427
Mammoth	0.006881	19.003116	12.485656	9.597256	7.467309	9.990367
Swiss roll	0.002085	9.990367	3.522110	1.299816	0.733597	1.388023
Sphere	0.005694	2.763791	2.985690	0.983152	0.877690	0.939784
Iris	0.000508	1.369776	4.061811	0.309516	0.180864	0.606335
Coil-20	0.129517	3.824632	4.862549	2.802890	3.041111	3.126181
MNIST	1.123673	319.183082	37.511525	71.488276	48.22733	102.376454
Fashion MNIST	1.156796	326.614965	47.136507	70.206722	47.103224	102.332053
Duo 4Eq scRNA-seq	0.052447	13.919151	14.205324	4.211889	2.761129	4.424303

## CONCLUSION

In conclusion, the CBMAP algorithm presents several advantages in the realm of dimensionality reduction. By preserving both global and local structures, it effectively retains the inherent relationships and patterns present in high-dimensional data, facilitating better interpretation and understanding. Additionally, CBMAP offers scalability, computational efficiency, and a parameter-free or reduced reliance on hyperparameters, making it suitable for handling large datasets in real-world applications.

However, it's essential to acknowledge the limitations of CBMAP. The algorithm relies on the k-means clustering algorithm, which assumes data to be normally distributed. While this works well for normally distributed data and can be further improved with normalization, it may not perform optimally for datasets with non-normal distributions, such as count data. In such cases, alternative clustering methods and membership functions may be more suitable, presenting an avenue for future research and development.

## ACKNOWLEDGEMENT

B.D. is supported by the Scientific and Technological Research Council of Turkey (TUBITAK) with project number:120C152

## REFERENCES

- [1] M. Li, H. Wang, L. Yang, Y. Liang, Z. Shang, H. Wan, Fast hybrid dimensionality reduction method for classification based on feature selection and grouped feature extraction, *Expert Syst. Appl.* 150 (2020) 113277. <https://doi.org/10.1016/j.eswa.2020.113277>.
- [2] H. Hotelling, Analysis of a complex of statistical variables into principal components, *J. Educ. Psychol.* 24 (1933) 417–441. <https://doi.org/10.1037/h0071325>.
- [3] R.A. Fisher, The use of multiple measurements in taxonomic problems, *Ann. Eugen.* 7 (1936) 179–188. <https://doi.org/10.1111/j.1469-1809.1936.tb02137.x>.
- [4] J. Kruskal, M. Wish, *Multidimensional Scaling*, SAGE Publications, Inc., 2455 Teller Road, Thousand Oaks California 91320 United States of America, 1978.
- [5] J.B. Tenenbaum, V. de Silva, J.C. Langford, A global geometric framework for nonlinear dimensionality reduction, *Science* 290 (2000) 2319–2323. <https://doi.org/10.1126/science.290.5500.2319>.
- [6] S.T. Roweis, L.K. Saul, Nonlinear dimensionality reduction by locally linear embedding, *Science* 290 (2000) 2323–2326. <https://doi.org/10.1126/science.290.5500.2323>.
- [7] Visualizing Data using t-SNE Laurens van der Maaten, Geoffrey Hinton 9 (2008) 2579–2605.
- [8] L. McInnes, J. Healy, N. Saul, L. Großberger, UMAP: Uniform Manifold Approximation and Projection, *J. Open Source Softw.* 3 (2018) 861. <https://doi.org/10.21105/joss.00861>.
- [9] E. Amid, M.K. Warmuth, TriMap: Large-scale dimensionality reduction using triplets, *ArXiv [Cs.LG]* (2019). <http://arxiv.org/abs/1910.00204>.
- [10] Y. Wang, H. Huang, C. Rudin, Y. Shaposhnik, Understanding how dimension reduction tools work: An empirical approach to deciphering t-SNE, UMAP, TriMAP, and PaCMAP for data visualization, *ArXiv [Cs.LG]* (2020). <http://arxiv.org/abs/2012.04456>.
- [11] Mammuthus primigenius (blumbach), 3d.si.edu (n.d.). <https://3d.si.edu/object/3d/mammuthus-primigenius-blumbach:341c96cd-f967-4540-8ed1-d3fc56d31f12> (accessed April 26, 2024).
- [12] Sklearn.Datasets.Make\_s\_curve, Scikit-Learn (n.d.). [https://scikit-learn.org/stable/modules/generated/sklearn.datasets.make\\_s\\_curve.html](https://scikit-learn.org/stable/modules/generated/sklearn.datasets.make_s_curve.html) (accessed April 26, 2024).
- [13] S. Marsland, *Machine Learning: An Algorithmic Perspective*, Chapter 6 (2014).
- [14] Manifold Learning methods on a severed sphere, Scikit-Learn (n.d.). [https://scikit-learn.org/stable/auto\\_examples/manifold/plot\\_manifold\\_sphere.html](https://scikit-learn.org/stable/auto_examples/manifold/plot_manifold_sphere.html) (accessed April 26, 2024).

- [15] S.A. Nene, S.K. Nayar, H. Murase, Columbia Object Image Library (COIL-20), Technical Report CU-CS-005-96, 1996.
- [16] L. Deng, The MNIST database of handwritten digit images for machine learning research, *IEEE Signal Process. Mag.* 29 (2012) 141–142. <https://doi.org/10.1109/msp.2012.2211477>.
- [17] H. Xiao, K. Rasul, R. Vollgraf, Fashion-MNIST: A novel image dataset for benchmarking machine learning algorithms, *ArXiv [Cs.LG]* (2017). <http://arxiv.org/abs/1708.07747>.
- [18] G.X.Y. Zheng, J.M. Terry, P. Belgrader, P. Ryvkin, Z.W. Bent, R. Wilson, S.B. Ziraldo, T.D. Wheeler, G.P. McDermott, J. Zhu, M.T. Gregory, J. Shuga, L. Montesclaros, J.G. Underwood, D.A. Masquelier, S.Y. Nishimura, M. Schnall-Levin, P.W. Wyatt, C.M. Hindson, R. Bharadwaj, A. Wong, K.D. Ness, L.W. Beppu, H.J. Deeg, C. McFarland, K.R. Loeb, W.J. Valente, N.G. Ericson, E.A. Stevens, J.P. Radich, T.S. Mikkelsen, B.J. Hindson, J.H. Bielas, Massively parallel digital transcriptional profiling of single cells, *Nat. Commun.* 8 (2017) 14049. <https://doi.org/10.1038/ncomms14049>.
- [19] H. Huang, Y. Wang, C. Rudin, E.P. Browne, Towards a comprehensive evaluation of dimension reduction methods for transcriptomic data visualization, *Commun. Biol.* 5 (2022) 719. <https://doi.org/10.1038/s42003-022-03628-x>.
- [20] A. Duò, M.D. Robinson, C. Soneson, A systematic performance evaluation of clustering methods for single-cell RNA-seq data, *F1000Res.* 7 (2018) 1141. <https://doi.org/10.12688/f1000research.15666.2>.